CrossMark

Adaptive neuro-fuzzy inference system-based grey time-varying sliding mode control for power conditioning applications

En-Chih Chang[1] · Rong-Ching Wu[1] · Ke ZHU[2] · Guan-Yu Chen[1]

Abstract This paper develops an adaptive neuro-fuzzy inference system-based grey time-varying sliding mode control (TVSMC) for the application of power conditioning systems. The presented methodology combines the merits of TVSMC, grey prediction (GP), and adaptive neuro-fuzzy inference system (ANFIS). Compared with classic sliding mode control, the TVSMC accelerates reaching phase and guarantees the sliding mode existence starting at arbitrary primary circumstance. But, as a highly nonlinear loading occurs, the TVSMC will undergo chattering and steady-state errors, thus degrading PCS's performance. The GP is therefore used to attenuate the chattering if the overestimate of system uncertainty bounds exists and to lessen steady-state errors if the underestimate of system uncertainty bounds happens. Also, the GP-compensated TVSMC control gains are optimally tuned by the ANFIS for achieving more precise tracking. Using the proposed methodology, the power conditioning system (PCS) robustness is increased expectably, and low distorted output voltage and fast transient response at PCS output can be achieved even under nonlinear loading. The analysis in theory, design process, simulations, and digital signal processing-based experimental realization for PCS are represented to support the efficacy of the proposed methodology. Because the proposed methodology is easier to implement than prior methodologies and provides high tracking accuracy and low computational complexity, the contents of this paper will be of interest to learners of correlated artificial intelligence applications.

Keywords Time-varying sliding mode control (TVSMC) · Grey prediction (GP) · Adaptive neuro-fuzzy inference system (ANFIS) · Chattering · Power conditioning system (PCS)

✉ En-Chih Chang
  enchihchang@isu.edu.tw

  Rong-Ching Wu
  rcwu@isu.edu.tw

  Ke ZHU
  zhuke@connect.hku.hk

  Guan-Yu Chen
  mynameguanguan@gmail.com

[1] Department of Electrical Engineering, I-Shou University, No.1, Sec. 1, Syuecheng Rd., Dashu District, Kaohsiung City 84001, Taiwan, ROC

[2] Department of Electrical and Electronic Engineering, The University of Hong Kong, Pokfulam Road, Pokfulam, Hong Kong

1 Introduction

Numerous power conditioning systems are widely seen in industry, such as photovoltaic energy systems, wind energy systems, and hydrogen fuel cell systems. The PCS performance depends on the inverter-LC filter unit, whose task is to transform the DC to AC voltages. Thus, the capability of promising low distorted PCS inverter output voltage under nonlinear loading and fast transient response under phase-controlled loading must be attained; this can be fulfilled by utilizing feedback control strategies. The PI control is frequently applied; but while the loading is highly nonlinear and uncertain, the low distorted output voltage and fast transient response cannot be obtained [1, 2]. Many advanced control technologies derived for power conditioning systems are also cited, such as deadbeat control, repetitive control, and mu-synthesis. As reported in [3], deadbeat control has been successfully applied to control PCS, but this method

depends on parameters exactness and PCS output waveform has a noticeable distortion. A multilevel PCS with the use of deadbeat control is presented in [4]; although the proposed system has good steady-state performance, this technique is complex and the transient response is unsatisfactory. A modified deadbeat control methodology is suggested for PCS. The system exhibits very fast dynamic response, but this methodology is sensitive to variations of plant parameter, leading to nonzero steady-state errors [5]. The deadbeat control with robust predictors is applied to the dual-loop regulation of the PCS. Although the scheme presents excellent dynamic response in transient phase of the PCS, the steady-state performance of this scheme with a nonlinear loading is somewhat mediocre [6]. The repetitive control associated with the concept of an adaption-type is proposed for PCS to perform zero steady-state errors and to lessen output voltage distortion in face of nonlinear loading. Nevertheless, such an algorithm suffers from complicated control algorithms [7]. The PCS output is developed by a simpler repetitive scheme, and it attenuates the harmonic components. This scheme has simple control structure and shows low output voltage distortion, but obtains poor transient response in the presence of nonlinear loading [8]. The mu-synthesis is proposed as a choice to PCS control since it resolves the problem of system uncertainties, but its complex algorithm makes digital realization difficult and the steady-state error occurs when the load is highly nonlinear [9, 10]. Sliding mode control (SMC) is inherently robust against internal parameter variations and external interferences [11, 12]. The SMC has displayed that it is a good choice of techniques in PCS design [13–18]. In [13], a reduced state feedback method for PCS is proposed. But, a conventional SMC is employed and such a method results in output voltage distortion in steady-state execution with a nonlinear loading. The tracking control scheme based on input–output feedback linearization SMC technique has also been adopted for PCS design. The high-quality output voltage cannot be seen between steady-state and transient state [14]. Reference [15] utilizes an integral sliding control law to achieve PCS tracking control. This method has poor dynamic response and an undesirable chattering phenomenon. The digital SMC with dual-loop in PCS design is presented [16]; the tracking trajectory runs away target sliding surface and therefore output voltage distortion exists in nonlinear loading. In the works of [17, 18], they adopt continuous-time SMC scheme suitable for power conditioning systems, showing fast dynamic and satisfactory steady state. Nevertheless, owing to nominal loading deviation, the reliability of the SMC deteriorates. As abovementioned [13–18], the lessened output voltage distortion and fast transient response in SMC design have been reported. But, these use fixed sliding surfaces. For classic SMC design with the fixed sliding surface, the sliding mode

exists while the tracking trajectory hits and keeps in the sliding surface. Therefore, a reaching phase indicates the trajectory from an arbitrary primary circumstance tending towards sliding surface; the trajectory is not robust to system interferences before the sliding mode happens [19, 20]. To solve such a problem, the TVSMC with the use of rotating and shifting from arbitrary primary circumstances tending towards the target sliding surface can be utilized. By applying the concept of TVSMC, the insensitivity to system uncertainties can be decreased through speeding up the reaching phase [21, 22]. But, if a highly nonlinear loading is applied, the chattering and steady-state errors will occur in TVSMC system, thus yielding severe output voltage distortion and even degrading PCS performance. The grey prediction (GP) has been successfully applied in a wide variety of fields. The GP without difficult computation and complex mathematical structure is capable of building a grey model by a few data sampling only that can precisely forecast serial system state [23–26]. This paper uses the GP with mathematically simple and arithmetically efficient GP for attenuating the chattering or steady-state errors if the overestimate or underestimate of system uncertainties bounds occurs. Additionally, an adaptive neuro-fuzzy inference system (ANFIS) associating the training ability of neural network with approximate human reasoning of fuzzy logic is popular artificial intelligence technique in many engineering areas [27–30]. The ANFIS assists in generating and optimizing the fuzzy membership functions as well as the fuzzy rules [31–35]. By such a hybrid learning technique, the error between desired and actual output can be minimized [36–39]. Thus, the ANFIS is employed to tune GP-compensated TVSMC control gains optimally so that more precise tracking control can be obtained. By combining TVSMC, GP, and ANFIS, the proposed methodology produces a closed-loop power conditioning system with low total harmonic distortion, fast transient response, chattering alleviation, and steady-state errors attenuation under various loadings. Simulations and experiments are finally shown to validate the performance of the proposed methodology. Section II presents the dynamic modelling of the power conditioning system. The proposed methodology is represented in section III. Sections IV and V represent the simulation and experimental results and conclusions, respectively.

2 System modelling

Figure 1 represents the structure of a static power supply, which can be used in power conditioning system. The LC filter and R can be regarded as a plant. The output voltage v_c of the plant has to be requested to follow an AC reference v_r, by the proposed methodology.
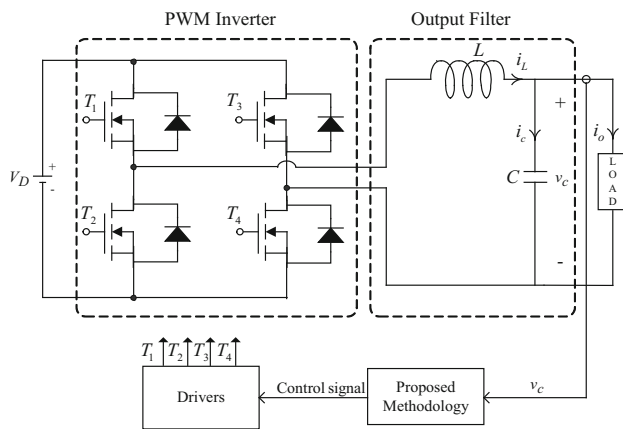
Fig. 1 Structure of power conditioning system

Fig. 2 Constitution of the proposed methodology using time-varying sliding surface

The plant can be written as

$$\dot{x}_p = A_p x_p + B_p u_p + d \qquad (1)$$

where $x_p = [x_{p1} \quad x_{p2}]^T = [v_c \quad \dot{v}_c]^T$, $A_p = \begin{bmatrix} 0 & 1 \\ -\dfrac{1}{LC} & -\dfrac{1}{RC} \end{bmatrix}$, $B_p = \begin{bmatrix} 0 \\ \dfrac{1}{LC} \end{bmatrix}$, u_p is the plant control input, and d is the interference.

The reference model with a sinusoidal reference frequency ω_0 can be represented as

$$\dot{x}_m = A_m x_m + B_m u_m \qquad (2)$$

where $x_m = [x_{m1} \quad x_{m2}]^T = [v_r \quad \dot{v}_r]^T$, $A_m = \begin{bmatrix} 0 & 1 \\ \omega_0^2 & 0 \end{bmatrix}$, $B_m = \begin{bmatrix} 0 \\ 1 \end{bmatrix}$, and u_m is the model control input.

Thus, the error differential equation yields

$$\begin{cases} e = x_m - x_p \\ \dot{e} = A_m e + (A_m - A_p)x_p + B_m u_m - B_p u_p - d \end{cases} \qquad (3)$$

The control goal is to design a control law u_p, and then the plant state x_p can follow the demanded control x_m specified by a reference model. The tracking error $e = x_m - x_p$ is therefore formulated to carry out the control aim. A control methodology has to be designed for driving the tracking error to zero between the model and the plant states. The control design is developed in the following.

3 Control design

3.1 Time-varying sliding mode control (TVSMC)

The time-varying sliding surface is designed as

$$s = \rho(t)e - \gamma(t) \qquad (4)$$

where $\rho(t) = Et + F$, $\gamma(t) = Gt + H$, and E, F, G, H are constants. The constitution of the proposed methodology by time-varying sliding surface is represented in Fig. 2.
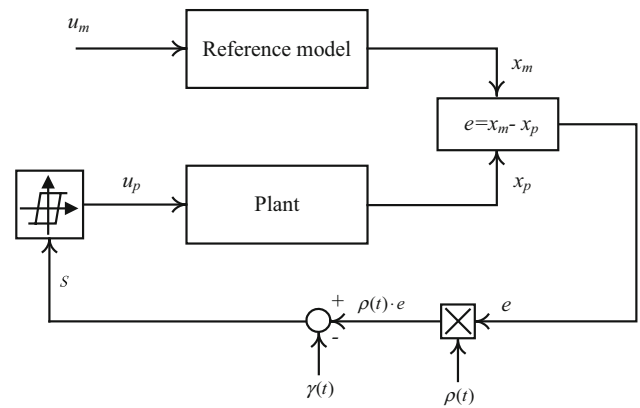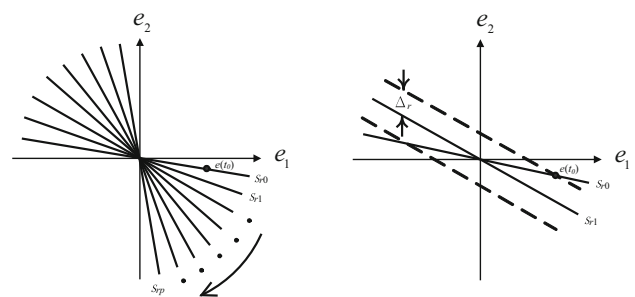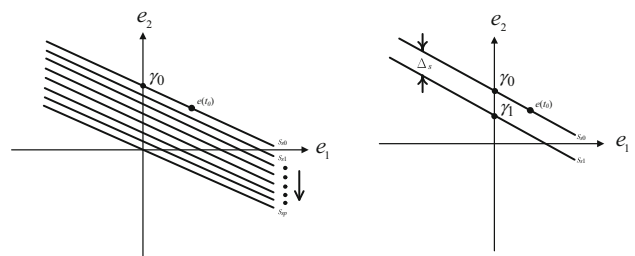

Fig. 3 RSS structure

Fig. 4 SSS structure

Figures 3 and 4 indicate that the time-varying sliding surface is composed of rotating sliding surface (RSS) and shifting sliding surface (SSS). The rotating and shifting can be operated by several ways. In the beginning the rotating or shifting relies on the primary state position. When the rotating is applied, the rotating will keep till the trajectory is convergent. When the shifting is applied, the surface is moved as this algorithm demands. Simultaneously, the feasibility of the rotating is checked. If it is feasible, the rotating will continue until the trajectory convergence. Even though the rotating is infeasible, the shifting can guarantee the state converged to the target surface and then move forward to the origin. The algorithms of the RSS and the SSS are outlined below.

Assume a system with primary circumstance $(e(t_0), \dot{e}(t_0))$ and let the target sliding surface be

$$s = \dot{e} + k_t e. \tag{5}$$

Rotating sliding surface: The primary sliding surface can be selected as

$$s = \dot{e}_0 + \rho_0 e_0 \tag{6}$$

where $\rho_0 = -\dot{e}(t_0)/e(t_0)$. The sliding surface can be decided as the following.

The new value ρ_{new} can be obtained by the sliding surface moving every Δ_τ second.

$$|s| = |\dot{e} + \rho_{new} e| = \Delta_r \tag{7}$$

where Δ_r must be small so that the system behaviour can maintain on the sliding surface, and a Δ_τ needs to be determined, thus moving the system from $s(t) = \Delta_r$ to $s(t + \Delta_\tau) = 0$. In (7), two solutions satisfy the ρ_{new}. When $\rho_0 > k_t$ or $\rho_0 < k_t$, the smaller or larger value of the ρ_{new} is applied, and the ρ is decreased or increased. When $\rho_0 < k_t$ or $\rho_0 > k_t$, the rotating stops under the circumstance of $\rho_{new} \geq k_t$ or $\rho_{new} \leq k_t$, and then $\rho_{new} = k_t$ is allowed.

Shifting sliding surface: When $e(t_0), \dot{e}(t_0) > 0$, the rotating is infeasible, incurring a non-Hurwitz sliding surface. The shifting with a sliding surface will pass through $e(t_0), \dot{e}(t_0)$, and then $\gamma_0 = \gamma(t_0)$. The $\gamma = 0$ must be obtained and the trajectory is converged to (7).

The new value γ_{new} can be chosen as

$$|s| = |\dot{e} + \rho e + \gamma_{new}| = \Delta_s \tag{8}$$

When $\gamma_0 < 0$ or $\gamma_0 > 0$, the larger or smaller value of the γ_{new} is applied, and the γ is increased or decreased. When $\gamma_0 > 0$ or $\gamma_0 < 0$, the shifting stops under the circumstance of $\gamma_{new} \leq 0$ or $\gamma_{new} \geq 0$, and then let $\gamma_{new} = 0$.

Differential sliding surface can be expressed as

$$\dot{s} = Ee_1 + \rho(t)\dot{e} + G \tag{9}$$

Substituting (3) into (9) gives

$$\begin{aligned}\dot{s} = Ee_1 + \rho(t) \times [A_m e + (A_m - A_p)x_p \\ + B_m u_m - B_p u_p - d] + G\end{aligned} \tag{10}$$

The control input is set as

$$u_p = u_e + u_s \tag{11}$$

where u_e indicates the equivalent control that allows the execution of requested sliding mode while system uncertainties are zero. The u_s represents the sliding control component that guarantees sliding mode existence and can remove system uncertainties.

The sliding control u_s is defined as

$$u_s = Ke + K_n \tag{12}$$

Then, the Lyapunov function can be expressed as

$$V = \frac{1}{2}ss^2 \tag{13}$$

By Lyapunov criterion, the control law u_p guarantees $\dot{V} = s\dot{s} < 0$ for satisfying sliding mode existence; thus, the system is asymptotically stable.

3.2 Grey prediction (GP)

The GM(2,1) is adopted to create a grey prediction model, and the grey modelling process is stated in the following.

Step 1: Collecting the original sample data sequence

$$x^{(0)} = \left\{ x^{(0)}(n), \quad n = 1, 2, \ldots, k \right\} \tag{14}$$

Step 2: Mapping generating operation (MGO)

The system data sequence may be positive or negative, and then the MGO is used to map the negative data to the related positive data.

$$x_{gy}^{(0)} = \left\{ x^{(0)}(n) + \text{BIAS}, \quad k = 1, 2, \ldots, n \right\} \tag{15}$$

where BIAS is a constant.

Step 3: Taking accumulated generating operation (AGO) for $x_{gy}^{(0)}$

$$x_{gy}^{(1)}(n) = \sum_{j=1}^{n} x_{gy}^{(0)}(j), \quad n = 1, 2, \ldots, k \tag{16}$$

Step 4: Constructing GM(2,1) model

The difference GP model can be written as

$$x_{gy}^{(1)}(n+2) + Px_{gy}^{(1)}(n+1) + Qx_{gy}^{(1)}(n) = 0 \tag{17}$$

where P and Q are the coefficients of the GM(2,1) that requires estimating their values.

Equation (17) can be rewritten as

$$\begin{bmatrix} -x_{gy}^{(1)}(n+1) & -x_{gy}^{(1)}(n) \end{bmatrix} \begin{bmatrix} P \\ Q \end{bmatrix} = \begin{bmatrix} x_{gy}^{(1)}(n+2) \end{bmatrix} \tag{18}$$

Letting $n = 1, 2, \ldots, k-2$ and (18) becomes

$$\begin{bmatrix} -x_{gy}^{(1)}(2) & -x_{gy}^{(1)}(1) \\ -x_{gy}^{(1)}(3) & -x_{gy}^{(1)}(2) \\ \vdots & \vdots \\ -x_{gy}^{(1)}(k-1) & -x_{gy}^{(1)}(k-2) \end{bmatrix} \begin{bmatrix} P \\ Q \end{bmatrix} = \begin{bmatrix} x_{gy}^{(1)}(3) \\ x_{gy}^{(1)}(4) \\ \vdots \\ x_{gy}^{(1)}(k) \end{bmatrix} \tag{19}$$

Assume $Y = \begin{bmatrix} x_{\text{gy}}^{(1)}(3) \\ x_{\text{gy}}^{(1)}(4) \\ \vdots \\ x_{\text{gy}}^{(1)}(k) \end{bmatrix}$, $B =$

$\begin{bmatrix} -x_{\text{gy}}^{(1)}(2) & -x_{\text{gy}}^{(1)}(1) \\ -x_{\text{gy}}^{(1)}(3) & -x_{\text{gy}}^{(1)}(2) \\ \vdots & \vdots \\ -x_{\text{gy}}^{(1)}(n-1) & -x_{\text{gy}}^{(1)}(n-2) \end{bmatrix}$, and $J = \begin{bmatrix} P \\ Q \end{bmatrix}$, then the

estimated parameters P and Q can be solved by the least square estimation method as follows:

$$J = [P, Q]^T = (B^T B)^{-1} B^T Y \tag{20}$$

The solution of (20) can be found by defining $x_{\text{gy}}^{(1)}(n) = \beta^n$, $x_{\text{gy}}^{(1)}(n+1) = \beta^{n+1}$, and $x_{\text{gy}}^{(1)}(n+2) = \beta^{n+2}$, and thus the following equation is obtained as

$$\beta^{n+2} + P\xi^{n+1} + Q\xi^n = \beta^n(\beta^2 + P\xi + Q) = 0 \tag{21}$$

The roots for satisfying (21) are given as

$$\begin{cases} \beta_1 = \dfrac{-P + \sqrt{P^2 - 4Q}}{2} \\ \beta_2 = \dfrac{-P - \sqrt{P^2 - 4Q}}{2} \end{cases} \tag{22}$$

Step 5: Taking IAGO

$$\hat{x}_{\text{gy}}^{(0)}(n) = \hat{x}_{\text{gy}}^{(1)}(n) - \hat{x}_{\text{gy}}^{(1)}(n-1) \tag{23}$$

Step 6: Inversing IMGO

Using IMGO for $\hat{x}_{\text{gy}}^{(0)}$, the forecasted value of the original data sequence $\hat{x}^{(0)}$ yields

$$\hat{x}^{(0)}(n+1) = \hat{x}_{\text{gy}}^{(1)}(n+1) - \hat{x}_{\text{gy}}^{(1)}(n) - \text{BIAS} \tag{24}$$

The control law of (11) can be restated as

$$u_{\text{p}}(n) = u_{\text{e}}(n) + u_{\text{s}}(n) + u_{\text{gy}}(n) \tag{25}$$

where the difference GP control, u_{gy} can remove the chattering or attenuate steady-state errors.

$$u_{\text{gy}}(n) = \begin{cases} 0, & |\hat{s}(n)| \leq \varepsilon \\ K_{\text{gy}}\hat{s}(n)\text{sgn}(s(n)\hat{s}(n)), & |\hat{s}(n)| \geq \varepsilon \end{cases} \tag{26}$$

where $\hat{s}(n)$ denotes the predicted value of $s(n)$ and ε represents the system boundary.

3.3 Adaptive neuro-fuzzy inference system (ANFIS)

Firstly, a Takagi–Sugeno (T–S) fuzzy structure is created by the ANFIS and then the given training data are modelled.

Then, the ANFIS is written as

Rule n : If e_1 is A_{n1} and e_k is A_{nk}
Then $u_n = p_{n1}e_1 + \cdots + p_{nk}e_k + r_n$ $\tag{27}$

where Rule n represents the nth fuzzy rules, $n = 1, 2, \ldots q$, A_{ni} denotes the fuzzy set in the antecedent associated with the ith input variable at the nth fuzzy rule, and $p_{n1}, \ldots p_{nk}$ and r_n are the fuzzy resulting parameters.

By the use of the ANFIS, the u_{p} can be obtained as

$$u_{\text{p}} = \frac{w_1}{w_1 + \cdots + w_{\text{q}}}u_1 + \cdots + \frac{w_{\text{q}}}{w_1 + \cdots + w_{\text{q}}}u_{\text{q}}$$
$$= \bar{w}_1 u_1 + \cdots + \bar{w}_{\text{q}} u_{\text{q}} \tag{28}$$

where $\bar{w}_1 = \frac{w_1}{w_1 + \cdots + w_q}$ and $\bar{w}_q = \frac{w_q}{w_1 + \cdots + w_q}$.

Owing to $u_n = p_{n1}e_1 + \cdots + p_{nk}e_k + r_n$, (28) can be restated as

$$\begin{aligned} u_{\text{p}} &= \bar{w}_1 u_1 + \cdots + \bar{w}_{\text{q}} u_{\text{q}} \\ &= (\bar{w}_1 e_1)p_{11} + \cdots + (\bar{w}_1 e_k)p_{1k} + \bar{w}_1 r_1 \\ &\quad + \\ &\vdots \\ &\quad + (\bar{w}_q e_1)p_{q1} + \cdots + (\bar{w}_q e_k)p_{qk} + \bar{w}_{\text{q}} r_{\text{q}} \end{aligned} \tag{29}$$

Equation (29) implies the proposed ANFIS with five-layer structure. More precisely, the concept of the neural network learning algorithm developed in [34] can directly be applied to (29). From the architecture of (29), it can be explored that when the values of premise parameters are given, the overall output can be written as a linear combination of the consequent parameters. More specifically speaking, in the forward pass of the ANFIS, functional signals move ahead till layer 4 and the consequent parameters are recognized by the least squares estimation; in the backward pass, the error rates propagate backward and the premise parameters are updated by the gradient descent method. Figure 5 displays the structure of the ANFIS and concisely summarizes the activities in each pass. The layer 1 represents for inputs, and every node is an adaptive node with a node function. The membership function for A can be any proper parameterized membership function. The layer 2 is for fuzzification, and every node is a fixed node labelled whose output is the product of all the incoming signals. Each node output denotes the firing strength of a rule. The layers 3 and 4 indicate for fuzzy rule evaluation. Every node of the layer 3 is a fixed node labelled N. The outputs of this layer are normalized firing strengths given, and in layer 4, every node is an adaptive node with a node function. Parameters in this layer are referred to as consequent parameters. The layer 5 denotes for defuzzification, and this layer with a fixed node
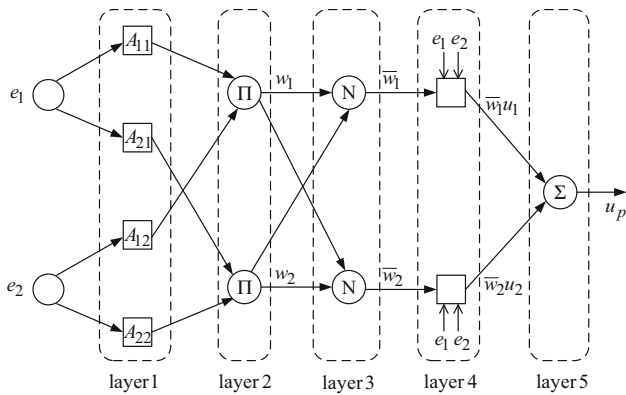
Fig. 5 Structure of the ANFIS

Fig. 7 Simulated waveforms under phase-controlled with the classic SMC (100 V/div; 30A/div; 5 ms/div)

labelled computes the overall output as the summation of all incoming signals.

4 Simulation and experimental results

To verify the effective operation of the proposed methodology, simulations and experiments are performed. The parameters of the PCS are given as follows: DC-bus voltage $V_D = 210$ V; output voltage $v_c = 110$ V; output frequency $f = 60$ Hz; filter inductor $L = 1.2$ mH; filter capacitor $C = 10$ μF; switching frequency $f_s = 12$ kHz; rated loading $R = 12\Omega$. Figures 6 and 7 show the simulated output voltage and the output current obtained using the proposed methodology and the classic SMC under phase-controlled loading from no load to $R = 12\Omega$ at a 90° firing angle every half cycle, respectively. As shown in Fig. 6, a close examination of the waveforms shows that there are a slight voltage droop and a rapid steady-state recovery. But, the voltage waveform shown in Fig. 7 achieves poor dynamic response and very visible period distortion. Evidently, as an abrupt loading disturbance is
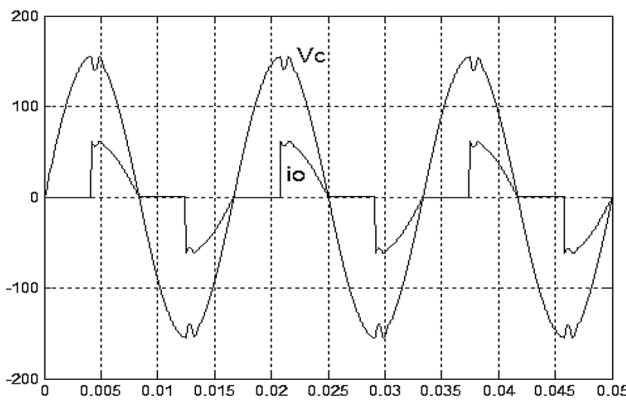
applied to the AC power conditioner, the proposed controller not only maintains the inherent robustness but has fast dynamic response. To test the performance of the AC power conditioner with the proposed methodology under nonlinear loading consisted of a full-wave diode bridge rectifier with an electrolytic capacitor of 200 μF and load resistance of 55Ω, the simulated output voltage and the output current waveforms are displayed in Fig. 8. The output voltage is very close to sinusoidal waveform with low THD (%THD equals 1.53 %), and high steady-state accuracy is obtained. Compared with the proposed methodology, the simulated waveforms obtained using the classic SMC under nonlinear loading are reported in Fig. 9. The high harmonic distortion exists in output voltage (%THD equals 9.04 %), thus yielding inaccurate steady-state response. Figure 10 displays the experimental output voltage and the output current with the proposed methodology under phase-controlled loading from no load to $R = 12\Omega$. As can be seen, a fast steady-state recovery is achieved. Nevertheless, the experimental waveform with the classic SMC shown in Fig. 11 has unsatisfactory voltage sag compensation. In addition, Figs. 12 and 13

Fig. 6 Simulated waveforms under phase-controlled loading with the proposed methodology (100 V/div; 30A/div; 5 ms/div)

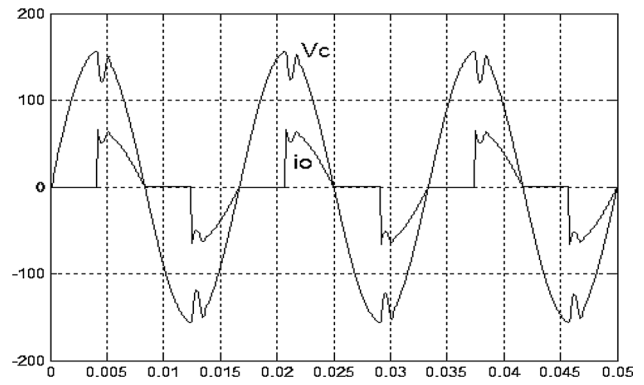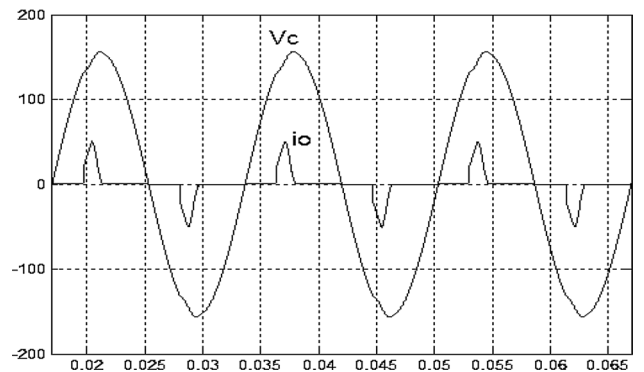**Fig. 8** Simulated waveforms under nonlinear loading with the proposed methodology (100 V/div; 30A/div; 5 ms/div)
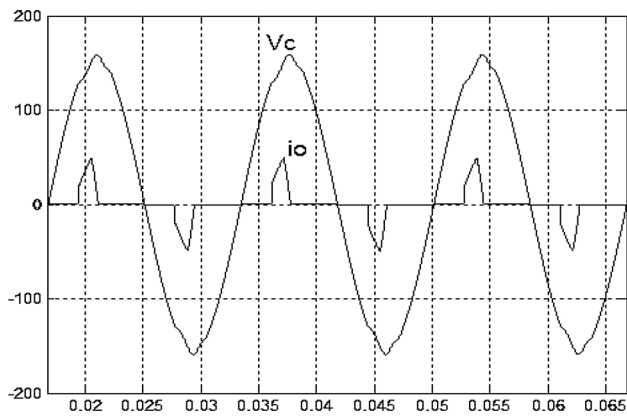
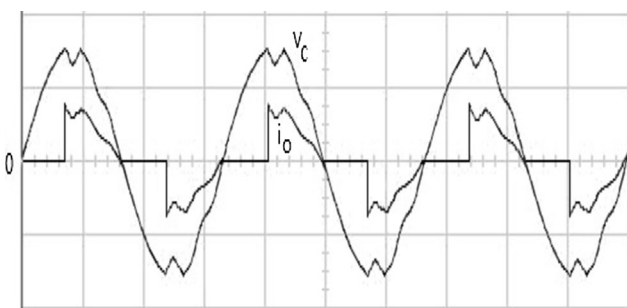**Fig. 9** Simulated waveforms under nonlinear loading with the classic SMC (100 V/div; 30A/div; 5 ms/div)

Fig. 10 Experimental waveforms under phase-controlled loading with the proposed methodology (100 V/div; 20A/div; 5 ms/div)
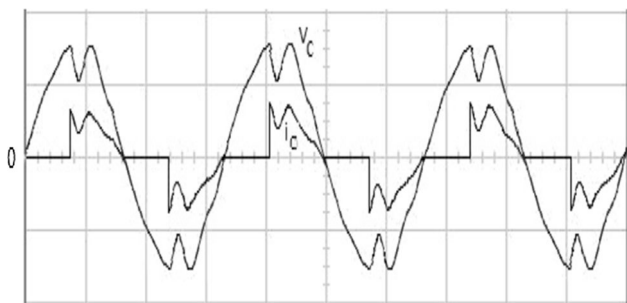

Fig. 11 Experimental waveforms under phase-controlled loading with the classic SMC (100 V/div; 20A/div; 5 ms/div)
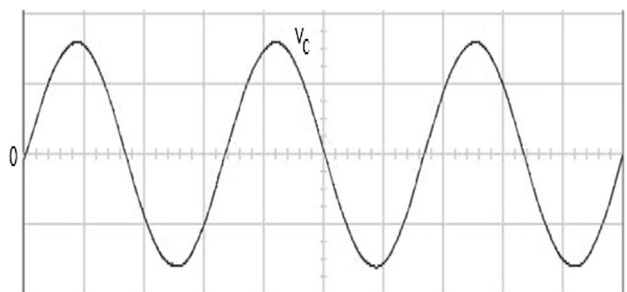

Fig. 12 Experimental waveforms under LC parameter variations with the proposed methodology (100 V/div; 5 ms/div)
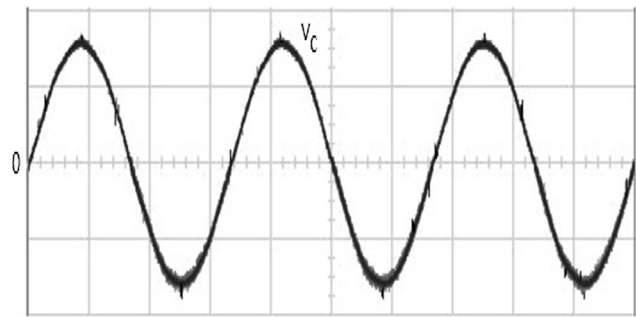

Fig. 13 Experimental waveforms under LC parameter variations with the classic SMC (100 V/div; 5 ms/div)

Table 1 Simulated and experimental output voltage %THD

Proposed methodology		
Sim.		
Loading	Phase-controlled loading	Nonlinear loading
%THD	1.62 %	1.53 %
Classic SMC		
Sim.		
Loading	Phase-controlled loading	Nonlinear loading
%THD	8.34 %	9.04 %
Proposed methodology		
Exp.		
Loading	Phase-controlled loading	LC parameter variations
%THD	1.71 %	0.39 %
Classic SMC		
Exp.		
Loading	Phase-controlled loading	LC parameter variations
%THD	8.84 %	10.52 %

compare the experimental output voltage waveforms of the power conditioning system controlled by the proposed methodology and the classic SMC under LC filter parameter values undergoing 50–250 % variations of 12Ω nominal resistive values. The proposed PCS is more insensitive to the parameter variations than the classic sliding mode controlled PCS. Table 1 displays the simulated and experimental output voltage THD values of the proposed controlled PCS and the classic SMC-controlled PCS under different loads. In final summation, it is well confirmed that the proposed methodology always gives better steady-state accuracy, lower waveform distortion, and quicker convergence rate under various loading conditions, as compared to the classic SMC. The proposed methodology is thus more suitable for use in PCS design.

5 Conclusions

An ANFIS-based grey compensated TVSMC is presented to increase the tracking behaviour of the PCS, even a severe interference is applied. The TVSMC can reduce the reaching phase and is robust to parameter variations and interferences, thus enhancing the robustness of the system. But, while the loading is highly nonlinear, the chattering and steady-state errors yield. For achieving high tracking accuracy, the GP is used to remove the chattering and attenuate steady-state errors, which exists in TVSMC. Moreover, using the ANFIS with reduced rule numbers, faster operation speed and without modifying membership function by conventional trial and error, the control gains of the TVSMC with GP can be optimally tuned. Simulations and DSP-based experiments show that low output voltage distortion, fast dynamic response, chattering reduction, and steady-state errors attenuation are achieved in the presented PCS under both linear loading and non-linear loading.

References

1. Shin HB, Park JG (2012) Anti-windup PID Controller with integral state predictor for variable-speed motor drives. IEEE Trans Ind Electron 59(3):1509–1516

2. Rasoanarivo I, Brechet S, Battiston A, Nahid-Mobarakeh B (2012) Behavioral analysis of a boost converter with high performance source filter and a fractional-order PID controller. In: Proceedings of IEEE international conference on industry applications society annual meeting, pp 1–6

3. Martin D, Santi E (2014) Autotuning of digital deadbeat current controllers for grid-tie inverters using wide bandwidth impedance identification. IEEE Trans Ind Appl 50(1):441–451

4. Wang C, Ooi BT (2015) Incorporating deadbeat and low-frequency harmonic elimination in modular multilevel converters. IET Gener Transm Distrib 9(4):369–378

5. Hu J, Zhu ZQ (2013) Improved voltage-vector sequences on dead-beat predictive direct power control of reversible three-phase grid-connected voltage-source converters. IEEE Trans Power Electron 28(1):254–267

6. Chen Y, Luo A, Shuai Z, Xie S (2013) Robust predictive dual-loop control strategy with reactive power compensation for single-phase grid-connected distributed generation system. IET Power Electron 6(7):1320–1328

7. Herran MA, Fischer JR, Gonzalez SA, Judewicz MG, Carugati I, Carrica DO (2014) Repetitive control with adaptive sampling frequency for wind power generation systems. IEEE J Emerg Select Top Power Electron 2(1):58–69

8. Yan QZ, Wu XJ, Yuan XB, Geng YW (2016) An improved grid-voltage feedforward strategy for high-power three-phase grid-connected inverters based on the simplified repetitive predictor. IEEE Trans Power Electron 31(5):3880–3897

9. Chen Z, Yao B, Wang Q (2015) Mu-synthesis-based adaptive robust control of linear motor driven stages with high-frequency dynamics: a case study. IEEE/ASME Trans Mechatron 20(3):1482–1490

10. Bevrani H, Feizi MR, Ataee S (2016) Robust frequency control in an islanded microgrid: h-infinity and mu-synthesis approaches. IEEE Trans Smart Grid 7(2):706–717

11. Shtessel Y, Edwards C, Fridman L, Levant A (2014) Sliding mode control and observation. Springer, New York

12. Liu JK, Wang XH (2012) Advanced sliding mode control for mechanical systems design, analysis and MATLAB simulation. Springer, Heidelberg

13. Gudey SK, Gupta R (2015) Reduced state feedback sliding-mode current control for voltage source inverter-based higher-order circuit. IET Power Electron 8(8):1367–1376

14. Rezaei MM, Soltani J (2015) Robust control of an islanded multi-bus microgrid based on input–output feedback linearisation and sliding mode control. IET Gener Transm Distrib 9(15):2447–2454

15. Kang SW, Kim KH (2015) Sliding mode harmonic compensation strategy for power quality improvement of a grid-connected inverter under distorted grid condition. IET Power Electron 8(8):1461–1472

16. Vidal-Idiarte E, Marcos-Pastor A, Garcia G, Cid-Pastor A, Martinez-Salamero L (2015) Discrete-time sliding-mode-based digital pulse width modulation control of a boost converter. IET Power Electron 8(5):708–714

17. Montoya DG, Ramos-Paja CA, Giral R (2016) Improved design of sliding-mode controllers based on the requirements of MPPT techniques. IEEE Trans Power Electron 31(1):235–247

18. More JJ, Puleston PF, Kunusch C, Fantova MA (2015) Development and implementation of a supervisor strategy and siding mode control setup for fuel-cell-based hybrid generation systems. IEEE Trans Energy Convers 30(1):218–225

19. Tan SC, Lai YM, Tse CK (2012) Sliding mode control of switching power converters: techniques and implementation. CRC Press, Boca Raton

20. Azar AT, Zhu QM (2015) Advances and applications in sliding mode control systems. Springer, Heidelberg

21. Geng J, Sheng YZ, Liu XD (2013) Second-order time-varying sliding mode control for reentry vehicle. Int J Intell Comput Cybern 6(3):272–295

22. Li L, Zhang QZ, Rasol N (2011) Time-varying sliding mode adaptive control for rotary drilling system. J Comput 6(3):564–570

23. Liu S, Lin Y (2010) Advances in grey systems research. Springer, Heidelberg

24. Chang GW, Lu HJ (2012) Forecasting flicker severity by grey predictor. IEEE Trans Power Deliv 27(4):2428–2430

25. Saremi S, Mirjalili SZ, Mirjalili SM (2015) Evolutionary population dynamics and grey wolf optimizer. Neural Comput Appl 26(5):1257–1263

26. Ren WH, Lu ZM (2016) Link importance evaluation based on gray relational analysis for communication networks. J Netw Intell 1(1):38–45

27. Kass E, Eden T, Brown N (2014) Analysis of neural data. Springer, New York

28. Syropoulos A (2014) Theory of fuzzy computation. Springer, New York

29. Wang GY, Guan BL (2015) Fuzzy adaptive variational Bayesian unscented Kalman filter. J Inf Hiding Multimed Signal Process 6(4):740–749

30. Chen SM, Chang YC, Pan JS (2013) Fuzzy rules interpolation for sparse fuzzy rule-based systems based on interval type-2 Gaussian fuzzy sets and genetic algorithms. IEEE Trans Fuzzy Syst 21(3):412–425

31. JessiSahayaShanthi L, Arumugam R, Taly YK (2012) A novel rotor position estimation approach for a 8/6 solid rotor switched reluctance motor. Neural Comput Appl 21(3):461–468

32. Uddin MN, Huang ZR, Hossain AB (2014) Development and implementation of a simplified self-tuned neuro–fuzzy-based IM drive. IEEE Trans Ind Appl 50(1):51–59

33. Chairez I (2013) Differential neuro-fuzzy controller for uncertain non-linear systems. IEEE Trans Fuzzy Syst 21(2):369–384

34. Jang JSR, Sun CT, Mizutani E (2015) Neuro-fuzzy and soft computing: a computational approach to learning and machine intelligence. Pearson Education, New Delhi

35. Rahmani R, Langeroudi NMA, Yousefi R, Mahdian M, Seyedmahmoudian M (2014) Fuzzy logic controller and cascade inverter for direct torque control of IM. Neural Comput Appl 25(3–4):879–888

36. Wang XX, Ma LY (2014) A compact K nearest neighbor classification for power plant fault diagnosis. J Inf Hiding Multimed Signal Process 5(3):508–517

37. Tsai PW, Alsaedi A, Hayat T, Chen CW (2016) A novel control algorithm for interaction between surface waves and a permeable floating structure. China Ocean Eng 30(2):161–176

38. Lin CM, Leng CH, Hsu CF, Chen CH (2009) Robust neural network control system design for linear ultrasonic motor. Neural Comput Appl 18(6):567–575

39. Tsai PW, Chen CW (2014) A novel criterion for nonlinear time-delay systems using LMI fuzzy Lyapunov method. Appl Soft Comput 25:461–472